Investigation of the Ionic Conduction Mechanism of Polyether/Li$_7$La$_3$Zr$_2$O$_{12}$ Composite Solid Electrolytes by Electrochemical Impedance Spectroscopy

View the article online for updates and enhancements.

Investigation of the Ionic Conduction Mechanism of Polyether/Li₇La₃Zr₂O₁₂ Composite Solid Electrolytes by Electrochemical Impedance Spectroscopy

Masaki Kato, Koji Hiraoka, and Shiro Seki[*,z]

Graduate School of Applied Chemistry and Chemical Engineering, Kogakuin University, Hachioji, Tokyo 192-0015, Japan

Polyether-based polymer/cubic $Li_7La_3Zr_2O_{12}$ (LLZO) composite solid electrolytes were prepared by dispersing LLZO powder in a lithium (Li) conductive polyether-based solid polymer electrolyte. [SUS | electrolyte | SUS] (SUS: stainless steel) and [Li | electrolyte | Li] symmetrical cells were fabricated, and the ionic conductivity, Li/electrolyte interfacial resistance, and Li-cation transport number of the electrolytes were evaluated by electrochemical impedance spectroscopy. The polyether-based polymer/LLZO composite solid electrolytes showed relatively high ionic conductivity of over 10^{-4} S cm^{-1} at 333.15 K, along with high electrochemical stability and low interfacial resistance to Li metal electrodes. Remarkable changes of Cole-Cole plots were observed with the variation of LLZO content, which was attributed to the formation of local percolation pathways between LLZO grains in the polymer matrix. Li-ion conduction was faster in the LLZO phase than in the polymer phase. The Li-cation transport number of the polymer/LLZO composite solid electrolytes was almost constant value regardless of LLZO content because of the rate-limiting ionic transport in the polymer phase with a low Li-cation transport number.

Supplementary material for this article is available online

Lithium-ion secondary batteries (LIBs) are desired for use in not only portable devices and electric vehicles but also energy storage devices because of their high energy density and good cycle performance.[1–3] In general, carbonate-based organic solvents have been used as liquid electrolytes in conventional LIBs. However, there are risks associated with carbonate-based organic solvents and improvement of the safety of LIBs is very important for upsizing of LIBs for industrial applications. Considering this background, all-solid-state Li secondary batteries (ASSBs) containing non-flammable solid electrolytes are strongly desired. ASSBs are promising to not only solve the safety problems of conventional LIBs using liquid electrolyte, but also achieve high energy density by using a lithium (Li) metal negative electrode and cell stacking.[4,5]

For practical applications of high-performance ASSBs, it is important to thin the solid electrolyte layer to minimize the total cell resistance. Therefore, developing of solid electrolytes that possess not only high Li-ion (Li$^+$) conductivity, but also high mechanical strength in the thin film state (thickness: <100 μm) and good interfacial formability to various electrodes including Li metal anodes is required. Inorganic (oxide and sulfide) solid electrolytes and polymer electrolytes are suitable candidate materials as electrolytes for ASSBs.[6,7] Various oxide-based inorganic solid electrolytes have been reported to date including $(La,Li)TiO_3$ (LLTO) with perovskite structure,[8] $Li_{1.5}Al_{0.5}Ge_{1.5}(PO_4)_3$ (LAGP) with NASICON structure[9] and $Li_7La_3Zr_2O_{12}$ (LLZO) with garnet structure.[10,11] In particular, LLZO exhibits relatively high ionic conductivity of above 10^{-4} S cm^{-1} at room temperature and chemical stability to Li metal anodes, making it as attractive candidate material for use as an oxide-based solid electrolyte.[12] However, ceramic-based electrolytes have high electrolyte resistance because of the presence of grain boundaries, poor mechanical properties in the thin film state, and do not easily form a stable interface with an electrode. These problems lead to brittle failure of the electrolyte and high interfacial resistance between the electrolyte and electrodes, presenting a major bottleneck in the realization of high-performance ASSBs.

Solid polymer electrolytes that contain polyether (e.g., poly(ethylene)oxide, PEO) in the main chain and dissolved Li$^+$ as a carrier in the polymer matrix can form thin films with favorable mechanical properties and easily form stable interfaces with both cathodes and Li metal anodes because of their high flexibility and self-supporting ability.[13,14] However, the ionic conductivity of PEO-based electrolytes is relatively low of the order of 10^{-6} S cm^{-1} at room temperature compared with those of organic liquid electrolytes and inorganic solid electrolytes. Therefore, the performance of PEO-based electrolytes is not sufficient for their use as the electrolyte layer of ASSBs. The low ionic conductivity of PEO-based polymer electrolytes at room temperature is attributed to the dominant Li$^+$ conduction in the polymer electrolyte coupling with the thermodynamic relaxation motion of polymer segments. Li$^+$ dissolved in the polymer matrix can form pseudo cross-linked structures through to ion-dipole interactions with oxygen bonded in the polymer main or side chain. Therefore, Li$^+$ conduction in the system strongly depends on the thermodynamic motion of segments involved in the transient cross-linked structure, which leads to relative low conductivity.[15,16]

Against such a background, polymer/inorganic composite solid electrolytes combining two kind of materials have recently begun to attract attention.[17] The challenge is to realize a solid electrolyte that has both the high Li$^+$ conductivity of an inorganic electrolyte and high self-supporting ability and interfacial formability to electrodes of a polymer electrolyte by dispersing inorganic particles with high ionic conductivity into a flexible polyether-based polymer electrolyte. A composite electrolyte of LLZO particles in a polymer matrix with high ionic conductivity has been obtained.[18,19] However, decreased ionic conductivity upon composite formation has also been reported. The dominant factors affecting the ionic conduction of polymer/inorganic composite solid electrolytes are still not clear.[20–22]

Recently, the ionic conduction mechanism of a polymer/inorganic composite system was elucidated using solid-state NMR spectroscopy and an ionic conduction model.[23–26] Electrochemical impedance spectroscopy (EIS) is a useful electrochemical measurement method that detects electrical resistance in various circuits by applying an alternating current (AC) while varying frequency. The separation of resistance components that respond to different

*Electrochemical Society Member.
zE-mail: shiro-seki@cc.kogakuin.ac.jp

frequencies and the change of ionic conduction properties can be estimated from the changes of Nyquist (Cole-Cole) plots. Although the ionic conductivity of polymer/inorganic (LLZO) composite solid electrolytes has reported, the interfacial behavior between the electrolytes and Li electrodes and the ionic conduction mechanism in such composite systems have not been reported. In this study, we clearly separate the components attributed to bulk resistance, grain boundary resistance, and electrolyte/Li interfacial resistance and investigate the ionic conduction mechanism of polymer/LLZO composite systems using EIS measurements.

Experimental

Preparation of polyether/LLZO composite electrolytes.—All sample preparations were conducted in a dry argon-filled glovebox ($[O_2] < 10$ ppm, dewpoint < 193.15 K, Miwa Mfg Co., Ltd.). The polyether/LLZO composite electrolytes were prepared by photo-initiated polymerization using 2,2 dimethoxy-2-phenylacetophenone (DMPA) as a photo initiator from P(EO/PO) acrylate macromonomer (EO: ethylene oxide, PO: propylene oxide, ratio of EO:PO = ca. 8:2, M_w: ca. 8,000, Dai-ich Kogyo Seiyaku Co.). P(EO/PO) was used as a matrix polymer for $LiN(SO_2CF_3)_2$ (LiTFSA, Solvay Co., Ltd). LiTFSA ([Li]/[O]=0.1 per mole of oxygen units of P(EO/PO)) and DMPA (0.1 wt% based on P(EO/PO)) were dissolved in a mixed solution and then submicron order cubic LLZO powder (Toshima Mfg Co. Ltd) was added in the solution at a weight ratio of P(EO/PO): LLZO = 1: x (x = 0.2, 0.33, 0.42, 0.5, 0.6, 0.66). Acetonitrile was added to obtain a homogeneous solution. Each homogeneous solution was dried under vacuum for 12 h to completely remove acetonitrile. The mixtures were spread between two glass plates separated by a Teflon sheet with a thickness of 0.1 or 0.5 mm and then cut out. Polyether/LLZO composite thin films (P(EO/PO)/ LiTFSA-LLZO) were fabricated by irradiation with ultraviolet light for 5 min to induce cross-linking of P(EO/PO).

Physical properties of polyether/LLZO composite electrolytes.—Cross-sectional images of P(EO/PO)/LiTFSA-LLZO films were investigated using scanning electron microscopy (SEM; JCM-6000, JEOL). Glass transition temperatures (T_g) of P(EO/PO)/ LiTFSA-LLZO electrolytes were measured by differential scanning calorimetry (DSC; Thermo plus EVO2 DSC8231, Rigaku) under a N_2 atmosphere. The P(EO/PO)/LiTFSA-LLZO film samples for DSC measurements were tightly sealed in Al pans in the dry glovebox. The DSC measurements were conducted by cooling the samples cooled to 173.15 K followed by heating to 298.15 K at cooling and heating rates of 10 K min^{-1}. T_gs values were determined as the middle point of the heat capacity change in DSC thermograms during the programmed heating step. The crystal structure of the LLZO powder and surface of P(EO/PO)/LiTFSA-LLZO electrolytes were analyzed using X-ray diffraction (XRD; Miniflex 600, Rigaku) with Cu Kα radiation (λ = 1.5406 nm), in the 2θ range from 10° to 100° (Fig. S1 is available online at stacks.iop.org/JES/167/070559/ mmedia).

Electrochemical properties of polyether/LLZO composite electrolytes.—The ionic conductivity (σ) of the P(EO/PO)/LiTFSA-LLZO electrolytes was measured by AC impedance spectroscopy (VSP, Bio Logic). P(EO/PO)/LiTFSA-LLZO electrolyte films were cut into circles with a diameter of 12 mmϕ, and sandwiched between two stainless steel (SUS) plates as blocking electrodes, and encapsulated in a measurement cell to prevent to exposure to air. The measurement frequency range was from 200 kHz to 50 mHz with 100 mV an amplitude at temperatures above 353.15 K. All samples were thermally equilibrated at each temperature for 1.5 h prior to AC impedance measurements.

AC impedance measurements using [Li | electrolyte | Li] symmetrical cells were carried out to investigate the chemical stability and temperature dependence of electrolyte/Li metal electrode interfacial resistance. The prepared P(EO/PO)/LiTFSA-LLZO electrolyte films were sandwiched between two Li metal electrodes and encapsulated 2032-type coin cells in the glovebox. The measurement frequency range was from 200 kHz to 10 mHz with an amplitude of 100 mV. The coin cells were stored in a thermostat maintained at 333.15 K and impedance spectra were measured every
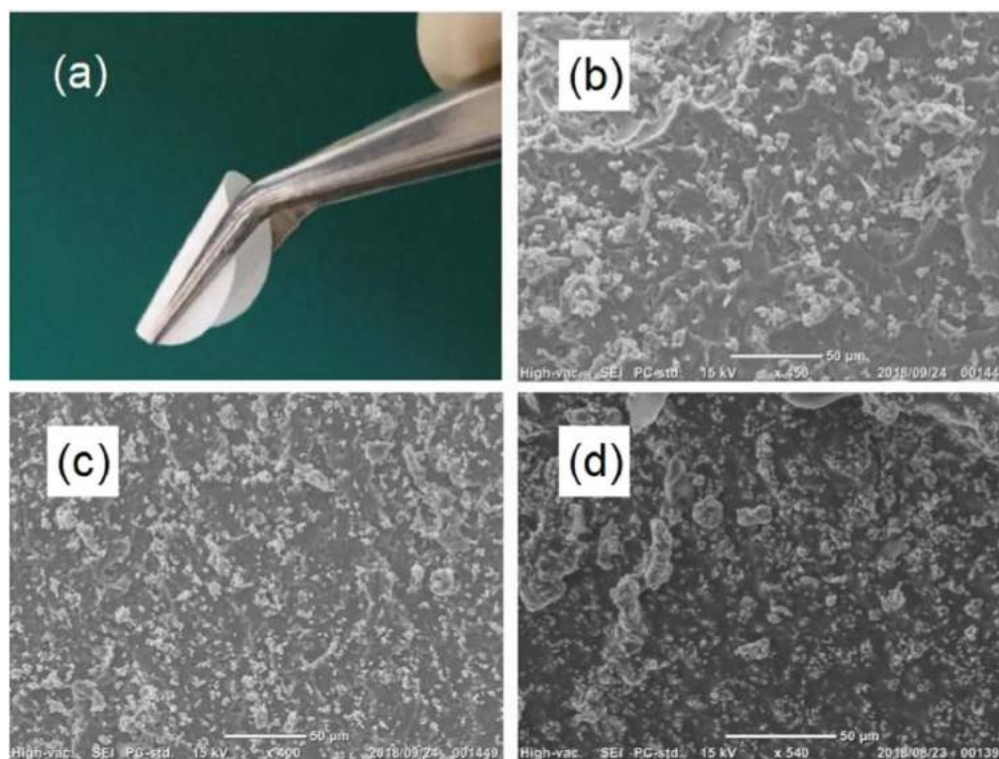
Figure 1. Appearance of the P(EO/PO)/LiTFSA-LLZO composite solid electrolyte (x = 0.5) (a). Cross-sectional SEM images of P(EO/PO)/LiTFSA-LLZO composites with (b) x = 0.42, (c) x = 0.5 and (d) x = 0.66.
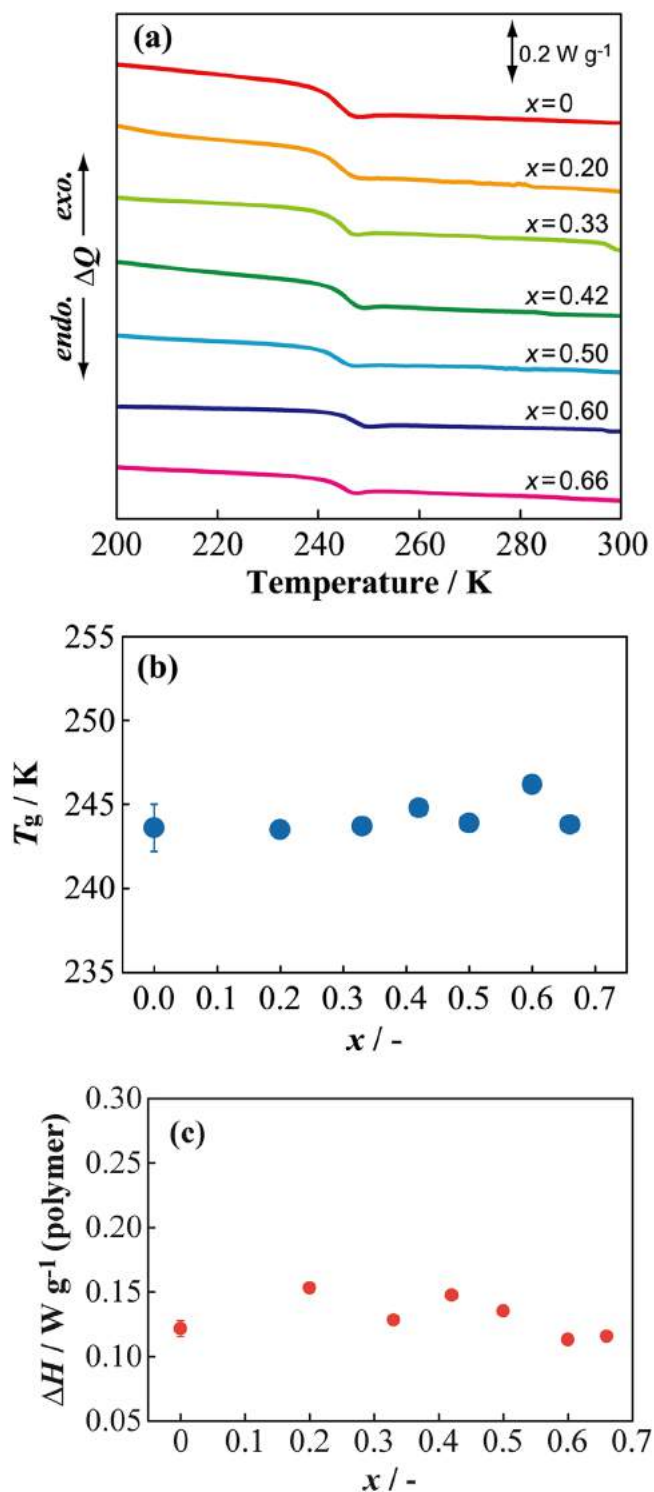
Figure 2. DSC thermograms (a), dependence of glass transition temperature (T_g) on LLZO concentration (b), and dependence of enthalpy changes of the glass transition (ΔH) on LLZO concentration (c) for P(EO/PO)/LiTFSA-LLZO composite electrolytes.

5 h. The temperature dependence of impedance spectra of samples were investigated by cooling from 353.15 K. The Li$^+$ transport number of polyether/LLZO composite solid electrolytes was measured by AC impedance spectroscopy using [Li | electrolyte | Li] symmetrical cells. The frequency range was from 200 kHz to 10 μHz with an amplitude of 10 mV and the measurement temperature was 333.15 K.
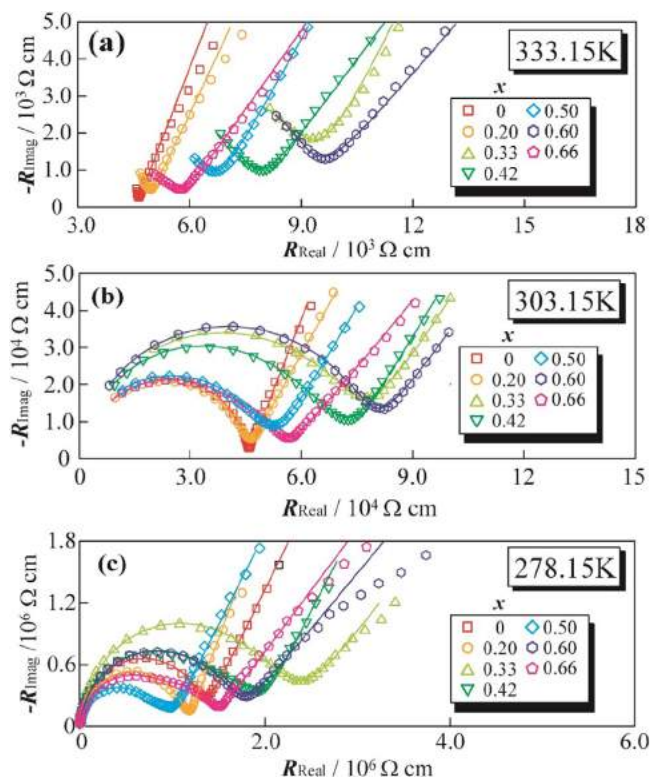
Figure 3. Cole-Cole plots of P(EO/PO)/LiTFSA-LLZO composite electrolytes using two SUS non-blocking electrodes at 278.15 (a), 303.15 (b) and 333.15 K (c).

Results and Discussion

Appearance and SEM image of polyether/LLZO composite solid electrolytes.—Figure 1a shows the appearance of the P(EO/PO)/LiTFSA-LLZO sample with $x = 0.33$ at room temperature. The sample was white because of the dispersed LLZO in the polymer matrix. Hybridization of an inorganic electrolyte with a polymer electrolyte is an approach to obtain inorganic-based solid electrolyte thin films without sintering. Polyether-based polymer electrolytes are attractive candidate material as genuine solid electrolyte to apply for ASSIBs owing to their high flexibility and mechanical property of thin film, compatibility with electrode and ease of cell assembly. P(EO/PO)/LiTFSA-LLZO composite solid electrolytes maintained high flexibility and self-standing properties even in thin films with a thickness of less than 100 μm in the samples with high LLZO content (>50 wt%, $x > 0.33$). Therefore, high compatibility with electrodes and good mechanical properties can be expected for the P(EO/PO)/LiTFSA-LLZO samples. Figures 1b–1d show SEM images of the cross section of P(EO/PO)/LiTFSA-LLZO thin films with different compositions. Aggregations of LLZO particles existed in the electrolyte film with a high LLZO content. Therefore, the density of local grain boundaries between LLZO particles was estimated to increase with LLZO content.

Thermal properties of polyether/LLZO composite solid electrolytes.—Figure 2a shows DSC thermograms of P(EO/PO)/LiTFSA-LLZO composite solid electrolytes during the heating process. In all films, a heat capacity change attributed to a thermal transition of the polymer electrolyte was observed at around 245 K. Apart from this clear thermal transition, no other peaks were observed. This heat capacity change should be caused by the glass transition of the polymer electrolytes. The T_g value of each P(EO/PO)/LiTFSA-LLZO electrolyte was determined from midpoint between values before and after the heat capacity change. Figure 2b presents the relationship between x and T_g for the P(EO/PO)/LiTFSA-LLZO samples. T_g of neat P(EO/PO)/LiTFSA ($x = 0$) was ca. 246 K. T_g of
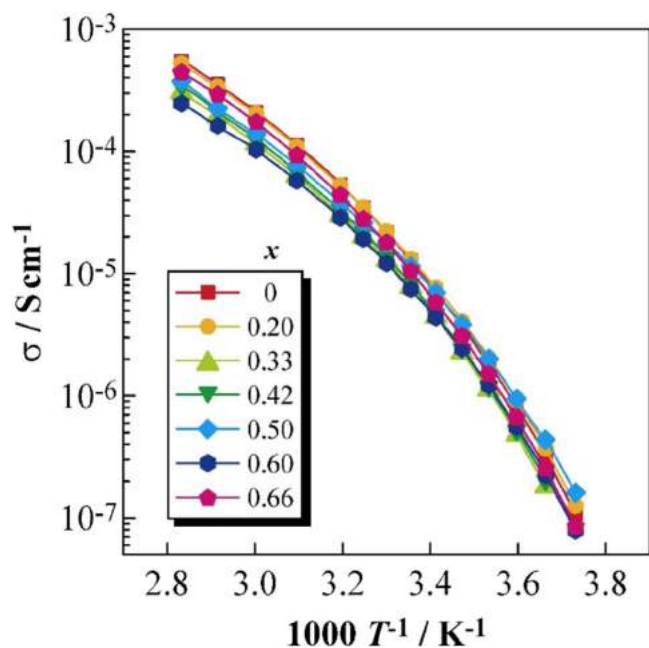
Figure 4. Arrhenius-type plots of the ionic conductivity of P(EO/PO)/LiTFSA-LLZO composite electrolytes.
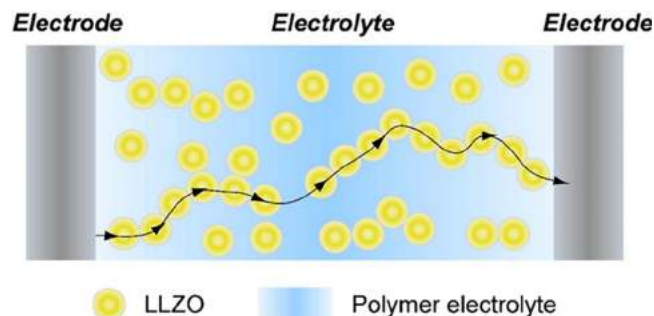
Figure 5. Schematic of the Li$^+$ conduction mechanism of P(EO/PO)/LiTFSA-LLZO composite electrolytes.

P(EO/PO)/LiTFSA-LLZO tended to increase slightly with rising LLZO content, but still remained fairly close to that of P(EO/PO)/LiTFSA. In general, dissolved Li$^+$ in a polyether-based matrix forms pseudo cross-linking points attributed to ion-dipole interactions between Li$^+$ and oxygen atoms in the polymer segments. Li$^+$ conduction in the electrolyte therefore occurs cooperatively with the local segmental motion of the polyether, which continuously forms and breaks pseudo cross-linking points. The interaction between incorporated LLZO particles and polymer electrolyte might be relatively weak because the LLZO in the polyether-based polymer electrolytes did not cause a remarkable increase of T_g. Figure 2c shows the relationship between the heat capacity change of the glass transition (ΔH) and x of the P(EO/PO)/LiTFSA-LLZO electrolytes. ΔH for each sample was calculated by removing the weight of polyether-based polymer in P(EO/PO)/LiTFSA-LLZO from the DSC thermogram as shown in Fig. 2a. ΔH of neat P(EO/PO)/LiTFSA was 0.14 W g^{-1}, and there was no strong correlation between ΔH and x of the P(EO/PO)/LiTFSA-LLZO electrolytes. This result indicates that effect of LLZO on the mobility of segments in the polymer matrix might be relatively weak.

Ionic conductive properties of polyether/LLZO composite solid electrolytes.—Figure 3 displays Cole-Cole plots of [SUS | P(EO/PO)/LiTFSA-LLZO | SUS] cells at 333.15 K (a), 303.15 K (b) and 278.15 K (c), respectively. Bulk resistance at high-frequency and a

straight line attributed to the diffusion component of the SUS electrode at low frequency were observed at 333.15 K. The equivalent circuit in Eq. 1 was used to analyze the Cole-Cole plots obtained at 333.15 K,

$$Q_b / R_b + Q_{diff.} \qquad [1]$$

where R_b is bulk resistance, Q_b is the capacitance of the electrolyte, and $Q_{diff.}$ is the capacitance of the diffusion element, respectively. A semicirclar arc derived from bulk resistance at high frequency and straight line attributed to diffusion in the SUS electrode at low frequency were observed at 303.15 K. While the impedance spectrum of P(EO/PO)/LiTFSA ($x = 0$) exhibited a highly symmetric semicirclar arc, those of the P(EO/PO)/LiTFSA-LLZO samples became more asymmetric with increasing x. This tendency was observed more clearly at low temperature (278.15 K). The increased asymmetry of the semicircular arc with increasing of x was attributed to the number of resistance components changing from one to more than one. Resistance attributed to grain boundaries between LLZO particles increased as the temperature decreased. This result indicated that a conductive phase of LLZO formed locally in the polymer phase at low temperature, and the effects of grain boundaries of LLZO were accentuated. The resistance components of bulk and grain boundaries were not able to be separated from the spectra using the equivalent circuit described by Eq. 1. Therefore, the following equivalent circuit containing added R_{GB} and Q_{GB} attributed to grain boundaries was used to analyze the obtained Cole-Cole plots,

$$Q_b / R_b + Q_{GB} / R_{GB} + Q_{diff.} \qquad [2]$$

where R_{GB} and Q_{GB} are the resistance and capacitance components of grain boundaries, respectively. The temperature dependence of R_{GB} calculated using the equivalent circuit described by Eq. 2 is shown in Fig. S2. R_{GB} increased linearly with decreasing temperature, but no clear correlation between R_{GB} and x was observed.

We succeeded in separating R_b, R_{GB} and R_{Li} from Cole-Cole plots of [Li | P(EO/PO)/LiTFSA-LLZO | Li] symmetrical cells and clarified the correlation between each resistance component and x by using Li metal as non-blocking electrodes instead of SUS blocking electrodes. These results allowed us to examine the relationship between R_{GB} and x in detail (*vide infra*). Figure 4 shows the temperature dependence of σ of P(EO/PO)/LiTFSA-LLZO calculated from sum of R_b and R_{GB} normalized by the thickness and apparent surface area of the electrolyte film. The σ values of P(EO/PO)/LiTFSA-LLZO exhibited the Vogel−Fulcher−Tammann (VFT) type temperature dependence,[27,28] which was derived from the characteristics of the amorphous ion-conductive polymer electrolyte. In addition, σ values of P(EO/PO)/LiTFSA-LLZO at each temperature were close to those of P(EO/PO)/LiTFSA, indicating that the rate of Li$^+$ conduction in the electrolytes was limited by the polymer phase. All σ values of P(EO/PO)/LiTFSA-LLZO at 333.15 K were about 10^{-4} S cm^{-1}, which makes them suitable for application as solid electrolytes in ASSBs.

Figure 5 shows a schematic of the ionic conduction mechanism of the P(EO/PO)/LiTFSA-LLZO electrolytes proposed from the EIS results. Li$^+$ in the P(EO/PO)/LiTFSA-LLZO electrolyte was conducted in both the polymer phase and LLZO phase. However, because both σ and the Li transport number of LLZO (t^+_{LLZO}) were much higher than those of the polymer phase (σ_{LLZO}(room-temperature): 10^{-3}–10^{-4} S cm^{-1}, $\sigma_{polymer}$(room-temperature): 10^{-6} S cm^{-1}, t^+_{LLZO}: ca. 1, $t^+_{polymer}$: 0.1–0.3), Li$^+$ should be preferentially conducted in the LLZO phase over the polymer phase. Comparing activation energies indicated that this tendency was more prominent at lower temperature. The proposed ion conduction model agrees well with that in a previous report.[23–26]
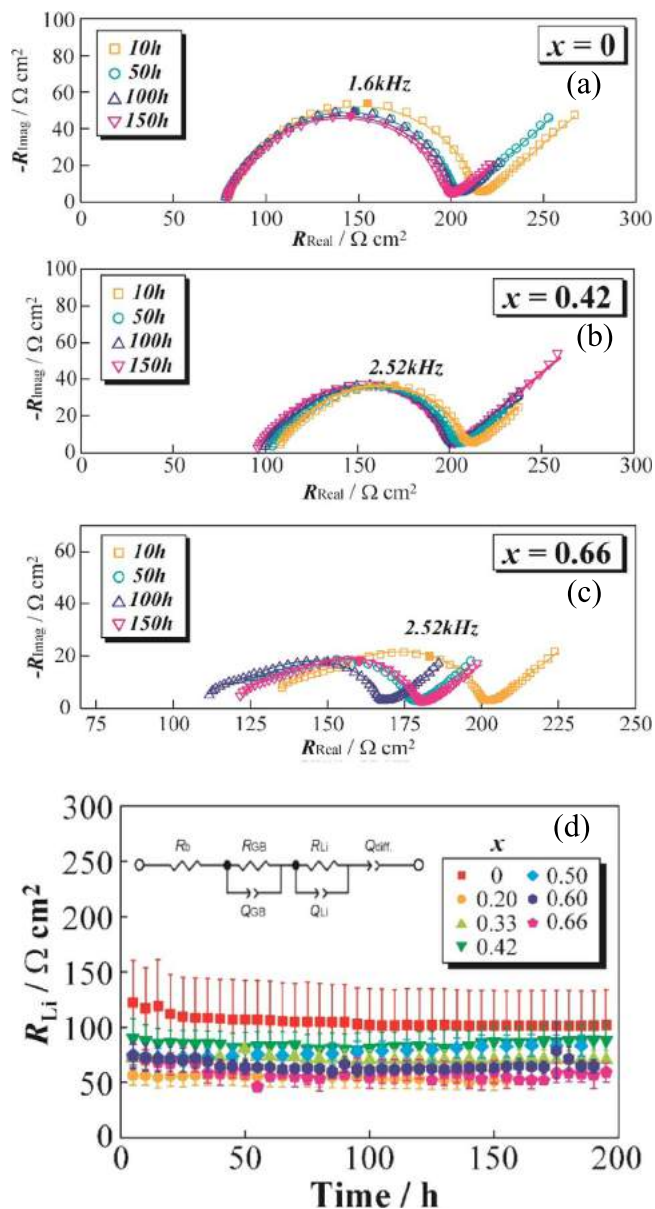
Figure 6. Time dependence of Cole-Cole plots of [Li | P(EO/PO)/LiTFSA-LLZO | Li] symmetrical cells at 333.15 K with (a) $x = 0$, (b) 0.42 and (c) 0.66), and time dependence of the electrolyte/Li metal interfacial resistance at 333.15 K (d).

[Li/polyether/LLZO composite solid electrolyte/Li] symmetrical cells.—Figure 6 shows time dependences of Cole-Cole plots for [Li | P(EO/PO)/LiTFSA-LLZO | Li] cells with $x = 0$ (a), 0.42 (b) and 0.66 (c), respectively, at 333.15 K. In Fig. 6a, the initial rise and symmetrical semicircle composed of R_b and R_{Li} attributed to bulk resistance and Li^+ charge transfer were observed in the low-frequency range. The diameter of this semicircular arc decreased as time elapsed, indicating the formation of a stable electrolyte/Li metal interface at relatively high temperature (333.15 K). These impedance spectra were analyzed using the equivalent circuit described by Eq. 3,

$$R_b + Q_{Li}/R_{Li} + Q_{diff.} \qquad [3]$$

where Q_{Li} and R_{Li} are capacitance and resistance components attributed to Li^+ charge transfer, respectively. Fitting of impedance spectra using Eq. 3 gave R_b and R_{Li} after 150 h of ca. 79 and 159 Ω cm², respectively. Cole-Cole plots of systems with $x = 0.42$ and 0.66

tended to show asymmetry because the linear part distorted faster than frequency over time. A concentrated LLZO phase formed in the electrolyte layer and R_{GB} attributed to this locally formed phase was assumed to increase in proportion to x, which is expected to induce changes of the Cole-Cole plots. The time constant of grain boundaries should be located between R_b and R_{Li} because a remarkable spectrum change occurred at higher frequency than the time constant of the semicircle of Li^+ charge transfer at the electrolyte/Li metal interface. Although impedance spectra of systems with up to $x = 0.42$ could be analyzed using Eq. 3, samples $x \geqslant 0.66$ could not be analyzed using this equivalent circuit. Therefore, we added further capacitance and resistance elements attributed to grain boundaries of LLZO,

$$R_b + Q_{GB}/R_{GB} + Q_{Li}/R_{Li} + Q_{diff.} \qquad [4]$$

Using Eq. 4, R_b and R_{Li} for the system with $x = 0.42$ after 150 h were calculated to be ca. 93 and 96 Ω cm², respectively. Similarly, R_b and R_{Li} for the system with $x = 0.66$ were calculated to be 117 and 60 Ω cm², respectively. Figure 6d shows the time dependence of R_{Li} of systems with each x at 333.15 K. R_{Li} decreased gradually over time and became almost constant. These results are consistent with the formation of a stable interface between P(EO/PO)/LiTFSA-LLZO and the Li metal electrodes 333.15 K. In general, polyether-based solid polymer electrolytes have been reported to form stable interfaces with Li anodes because of their high self-supporting ability and electrochemical stability.[29] Similarly, LLZO has been reported to form a stable interface with Li metal because of its high reductive stability.[7] Therefore, it is reasonable that polyether/LLZO composite electrolytes will also form stable interfaces with Li metal.[30] While the resistance values of the stable electrolyte/Li interface at 333.15 K were proportional to the reciprocal of exchange current density at the interface, resistance values for systems in the range of $x = 0.2–0.66$ tended to be lower than that with $x = 0$. Because Li ion transport number (τ_{Li+}) of polyether-based electrolytes is smaller than that of LLZO, the observed decrease of R_{Li} might be caused by the promotion of Li^+ charge transfer at the electrolyte/Li interface with increasing x.

Figure 7a shows Cole-Cole plots of [Li | P(EO/PO)/LiTFSA-LLZO | Li] symmetrical cells at 278.15 K. Both of R_b in the high-frequency range and R_{Li} at the electrolyte/Li metal interface in the low-frequency range were observed in the Cole-Cole plot of the system with $x = 0$. The time constants of R_b and R_{Li} were about 15.9 kHz and 8.9 Hz, respectively, calculated when this spectrum was fitted using the equivalent circuit described by Eq. 5,

$$Q_b/R_b + Q_{Li}/R_{Li} \qquad [5]$$

Another semicircular arc was observed at intermediate frequency range between those of bulk and Li^+ charge transfer at the electrolyte/Li metal interface with increasing x in the Cole-Cole plots of P(EO/PO)/LiTFSA-LLZO. This result clearly suggested that the formation of a percolation phase of LLZO particles in the electrolyte was promoted with x. These spectra were fitted using the equivalent circuit described by,

$$Q_b/R_b + Q_{GB}/R_{GB} + Q_{Li}/R_{Li} \qquad [6]$$

Figures 7b and 7c show the temperature dependence of R_{GB} and R_{Li}, as Arrhenius-type plots, which were analyzed by equivalent circuit described by Eq. 5. Both R_{GB} and R_{Li} increased linearly as temperature decreased. While R_{GB} at each temperature tended to increase with x, R_{Li} tended to decrease compared with that for the system with $x = 0$, similar to the results in Fig. 6d. The apparent activation energy (E_a) of each system was calculated using then Arrhenius equation. In general, the relationship between the rate of a chemical reaction and activation energy can be empirically expressed by the Arrhenius equation as follows,
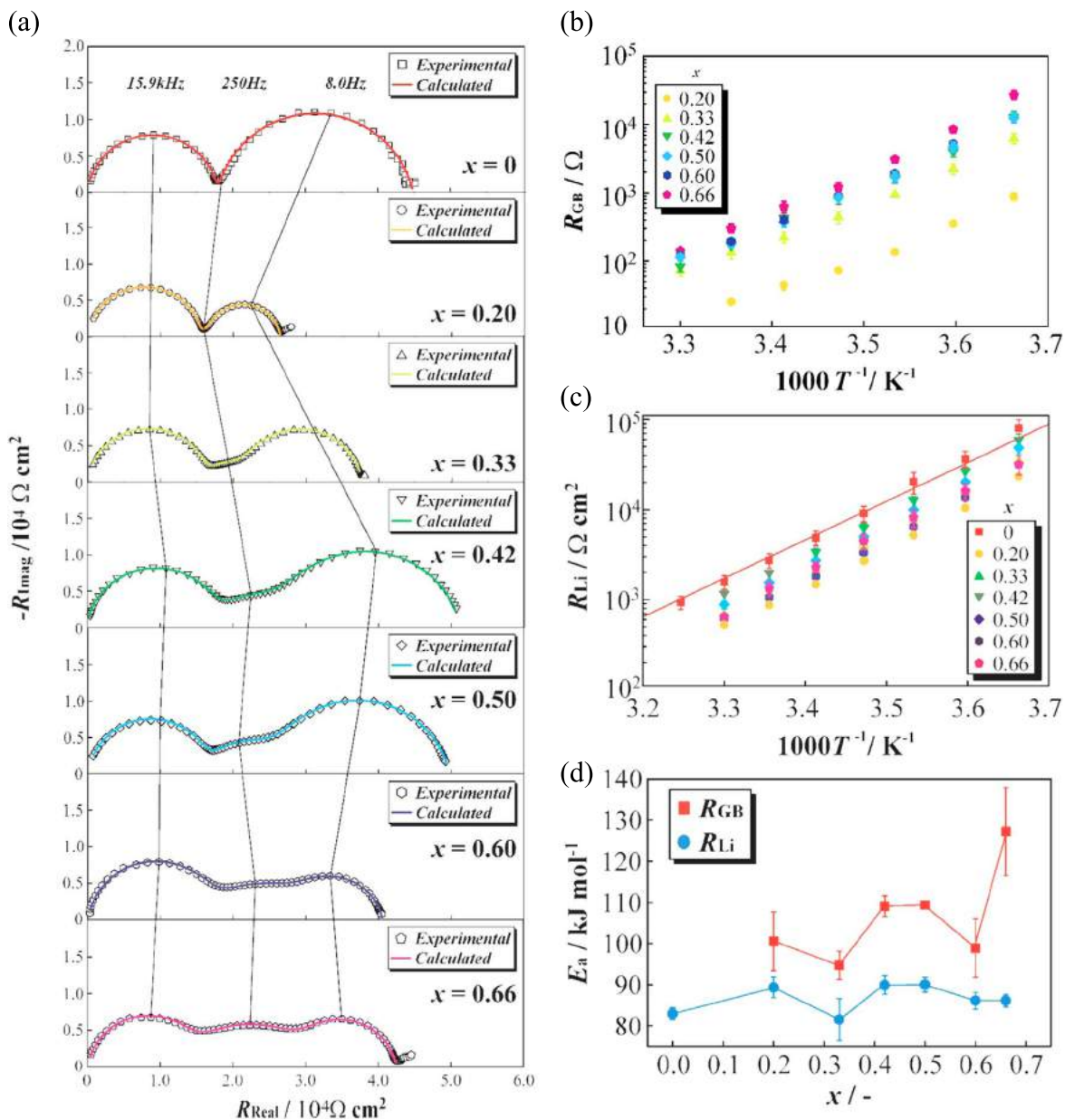
Figure 7. Cole-Cole plots of [Li | P(EO/PO)/LiTFSA-LLZO | Li] symmetrical cells at 278.15 K (a), temperature dependence of grain boundary resistances (b) and electrolyte/Li metal interfacial resistances (c) and dependence of the appearance activation energies of grain boundaries and electrolyte/Li metal interfacial resistance on x (d).

$$k = A \exp(E_a/RT) \qquad [7]$$

where k, A and R are the reaction rate constant, frequency factor and gas constant, respectively. If R_{GB} and R_{Li} are assumed to be proportional to the reciprocal of k, the relationships between each type of resistance and temperature can be expressed as follows,

$$R_{GB} = 1/k, \; R_{GB} = A' \exp(E_{a,GB}/RT) \qquad [8]$$

$$R_{Li} = 1/k, \; R_{Li} = A' \exp(E_{a,Li}/RT) \qquad [9]$$

where A' is the reciprocal of A. Equations 8 and 9 were applied to the data in Figs. 7b and 7c, allowing $E_{a,GB}$ and $E_{a,Li}$ to be calculated from the slope of each linear line. Figure 8d illustrates the relationship between calculated E_a values and x. $E_{a,GB}$ was always higher than $E_{a,Li}$. The dependence of $E_{a,Li}$ on x was relatively weak and $E_{a,Li}$ was almost constant at about 80 to 90 kJ mol^{-1}. It is suggested

that the decrease of R_{Li} was caused by the promotion of Li$^+$ charge transfer frequency at the Li metal interface. In contrast, $E_{a,GB}$ tended to increase with x. E_a of LLZO pellets was reported to be 0.36 eV (35.1 kJ mol^{-1}, at 291 to 323 K), which is much lower than our results. This discrepancy indicates that grain boundaries in the polyether/LLZO composite solid electrolytes were not the only source of resistance. In addition, Kun et al. reported that E_a of the interfacial resistance between LLZO and PEO was reported 96.5 kJ mol^{-1}.[31] This was similar value to the interfacial resistance of our polyether/LLZO composite electrolytes with x and this component was considered to be the rate-limiting process of ionic conduction in the electrolytes. E_a and the ionic conduction mechanism of polyether/inorganic composite electrolyte systems have been ever investigated by EIS and NMR spectroscopy.[23–26] However, clear separation of bulk, grain boundary, and interfacial resistance components using symmetrical non-blocking cells consisting of Li metal and polyether/LLZO composite solid electrolytes has not been reported elsewhere. The results of this study will aid
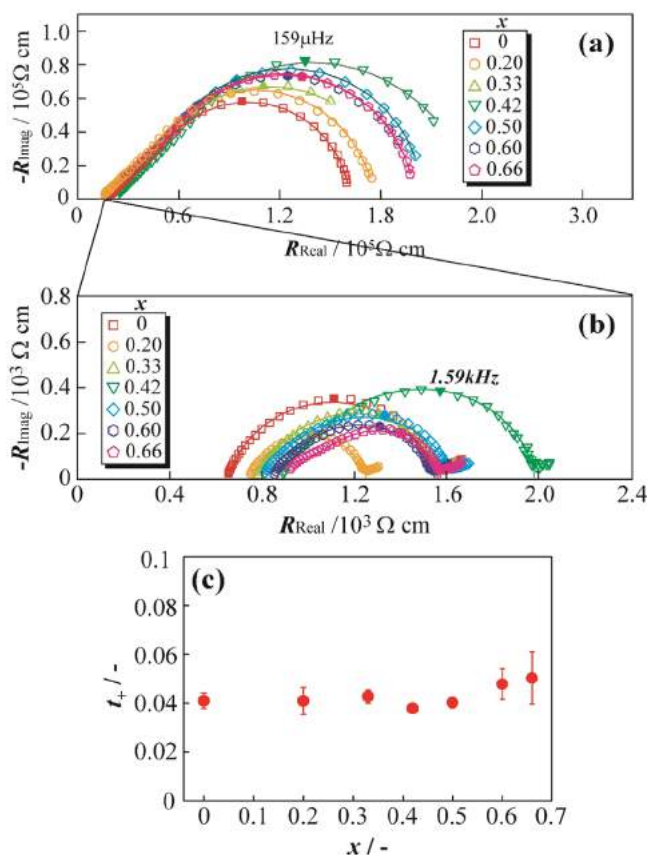
Figure 8. Cole-Cole plots of [Li | P(EO/PO)/LiTFSA-LLZO | Li] symmetrical cells at 333.15 K (a), (b), and dependences of the Li$^+$ transport number of P(EO/PO)/LiTFSA-LLZO composite electrolytes on x (c).

development of high-performance solid electrolytes using both organic and inorganic components.

Electrochemical Li$^+$ transport numbers of polyether/LLZO composite solid electrolytes.—Figure 8a shows Cole-Cole plots of [Li | P(EO/PO)/LiTFSA-LLZO | Li] symmetrical cells at 333.15 K and in the low-frequency region between 200 kHz and 10 mHz. Two semicircular arcs with vertex frequencies of 1.59 kHz and 159 μHz were observed. The first semicircular arc at higher frequency was attributed to the Li$^+$ charge transfer resistance between the electrolyte and Li metal because the time constant of this arc was close to those of the electrolyte/Li metal interface in Fig. 7. The second semicircular arc at low frequency was attributed to the resistance to Li$^+$ diffusion in P(EO/PO)/LiTFSA-LLZO. While the electrolyte with $x = 0$ showed a symmetrical semicircle at high frequency, the semicircular arcs at high frequency became more asymmetric with increasing x. This result correlated well with those in Fig. 7. The spectra in Fig. 8a were fitted by the equivalent circuits described as follows,

$$x = 0 \text{ to } 0.6 \qquad R_b + Q_{Li}/R_{Li} \qquad [10]$$

$$x = 0.66 \qquad R_b + Q_{GB}/R_{GB} + Q_{Li}/R_{Li} \qquad [11]$$

Experimental results and fitting results corresponded well. The semicircles at low frequency were fitted by the equivalent circuit described by Eq. 12, in which the sum of R_b and R_{Li} was replaced by R_{b+Li}.

$$x = 0 \text{ to } 0.66 \qquad R_{b+Li} + Q_{diff.}/Z_{diff.} \qquad [12]$$

where R_{b+Li}, $Q_{diff.}$ and $Z_{diff.}$ are the sum of R_b and R_{Li} and capacitance and resistance elements of Li diffusion, respectively. Experimental results and fitting results were also almost corresponded. Li$^+$ transport numbers (t_+) was calculated using the following equation,[32]

$$t_+ = R_b/(R_b + Z_{diff.}) \qquad [13]$$

Figure 8b shows the relationship between x and t_+ for the P(EO/PO)/LiTFSA-LLZO electrolytes. All t_+ values of the P(EO/PO)/LiTFSA-LLZO were quite low ($\sim$0.04). This result suggests that the rate of Li$^+$ conductions in the electrolytes was limited by the polymer phase and was also consistent with the similar ionic conductivities of P(EO/PO)/LiTFSA-LLZO and P(EO/PO)/LiTFSA electrolytes. To improve the ionic conductivity of polymer/inorganic composite electrolytes, it is important to increase the ionic conductivity of the polymer phase.

Conclusions

Polyether/Li$_7$La$_3$Zr$_2$O$_{12}$ (LLZO) composite solid electrolytes with high flexibility and electrochemical stability to Li metal electrodes were prepared with the aim of realizing high-performance ASSBs. The glass transition temperature, ionic conductivity, electrolyte/Li interfacial behavior and Li ionic transport number were investigated using thermal and electrochemical approaches. The polyether/LLZO composite solid electrolytes exhibited relative highly ionic conductivity of 10^{-4} S cm^{-1} at 333.15 K, which makes promising as electrolytes in ASSBs. EIS analysis of [Li | P(EO/PO)/LiTFSA-LLZO | Li] symmetrical cells revealed the contribution of LLZO grain boundaries to the electrolyte resistance. The EIS results also suggested that LLZO particles dispersed in the matrix formed a local percolation phase by dispersion and aggregation. The Li/electrolyte interfacial resistance tended to decrease with increasing LLZO concentration, which suggested increasing activity of Li$^+$ as a carrier ion near the interface of between the electrolyte and Li electrode. There are two possible paths for Li$^+$ conduction in the polyether/LLZO composite system; it was assumed that the preferential path was the LLZO phase because of its high ionic conductivity and theoretical Li$^+$ transport number of 1. Therefore, the ionic conductivity and Li$^+$ transport number of the polyether/LLZO composite system were similar value to those of the polyether-based polymer electrolyte because the rate of Li$^+$ conduction was limited by the polymer phase.

ORCID

Shiro Seki https://orcid.org/0000-0001-9717-2009

References

1. C. Sun, J. Liu, Y. Gong, D. P. Wilkinson, and J. Zhang, *Nano Ener.*, **33**, 363 (2017).
2. J. M. Tarascon and M. Armand, *Nature*, **414**, 359 (2001).
3. B. Dunn, H. Kamath, and J. M. Tarascon, *Science*, **334**, 928 (2011).
4. A. Manthiram, X. Yu, and S. Wang, *Nat. Rev. Mater.*, **2**, 16103 (2017).
5. F. Croce, G. B. Appetecchi, L. Persi, and B. Scrosati, *Nature*, **394**, 456 (1998).
6. L. Yue, J. Ma, J. Zhang, J. Zhao, S. Donga, Z. Liu, G. Cui, and L. Chen, *Energy Storage Mater.*, **5**, 139 (2016).
7. Q. Liu, Z. Geng, C. Han, Y. Fu, S. Li, Y. He, F. Kang, and B. Li, *J. Power Sources*, **389**, 120 (2018).
8. Y. Inaguma, C. Liquan, M. Itoh, T. Nakamura, T. Uchida, H. Ikuta, and M. Wakihara, *Solid State Commun.*, **86**, 689 (1993).

9. C. R. Mariappan, C. Yada, F. Rosciano, and B. Roling, *J. Power Sources*, **196**, 6456 (2011).

10. R. Murugan, V. Thangadurai, and W. Weppner, *Angew. Chem. Int. Ed.*, **46**, 7778 (2007).

11. V. Thangadurai, S. Narayanan, and D. Pinzaru, *Chem. Soc. Rev.*, **43**, 4714 (2014).

12. K. Fu et al., *Science Adv.*, **3**, e1601659 (2017).

13. L. Fan, S. Wei, S. Li, Q. Li, and Y. Lu, *Adv. Ener. Mater.*, **8**, 1702657 (2018).

14. S. Li. Long, M. Wang, Xiao, and Y. Meng, *J. Mater. Chem. A*, **4**, 10038 (2016).

15. S. Seki, M. A. B. H. Susan, T. Kaneko, H. Tokuda, A. Noda, and M. Watanabe, *J. Phys. Chem. B*, **109**, 3886 (2005).

16. A. Nishimoto, K. Agehara, N. Furuya, T. Watanabe, and M. Watanabe, *Macromolecules*, **32**, 1541 (1999).

17. C. Wang, Y. Yang, X. Liu, H. Zhong, H. Xu, Z. Xu, H. Shao, and F. Ding, *ACS Appl. Mater. Interfaces*, **9**, 13694 (2017).

18. K. Karthik and R. Murugan, *J. Solid State Electrochem.*, **22**, 2989 (2018).

19. F. Chen, D. Yang, W. Zha, B. Zhu, Y. Zhang, J. Li, Y. Gu, Q. Shen, L. Zhang, and D. R. Sadoway, *Electrochem. Acta*, **258**, 1106 (2017).

20. Z. Li, H. Huang, J. Zhu, J. Wu, H. Yang, L. Wei, and X. Guo, *ACS Appl. Mater. Interfaces*, **11**, 784 (2019).

21. F. Langer, I. Bardenhagen, J. Glenneberg, and R. Kun, *Solid State Ionics*, **291**, 8 (2016).

22. M. Keller, G. B. Appetecchi, G. Kim, V. Sharova, M. Schneider, J. Schuhmacher, A. Roters, and S. Passerini, *J. Power Sources*, **353**, 287 (2017).

23. J. Zagórski, J. M. L. Amo, M. J. Cordill, F. Aguesse, L. Buannic, and A. Llordés, *ACS Appl. Energy Mater.*, **2**, 1734 (2019).

24. J. Zheng and Y. Hu, *ACS Appl. Mater. Interfaces*, **10**, 4113 (2018).

25. T. Yang, J. Zheng, Q. Cheng, Y. Hu, and C. K. Chan, *ACS Appl. Mater. Interfaces*, **9**, 21773 (2017).

26. J. Zheng, M. Tang, and Y. Hu, *Angew. Chem. Int. Ed.*, **55**, 1 (2016).

27. H. Vogel, *Phys. Z.*, **22**, 645 (1921).

28. G. S. Fulcher, *J. Am. Ceram. Soc.*, **8**, 339 (1923).

29. G. B. Appetecchi, S. Scaccia, and S. Passerini, *J. Electrochem. Soc.*, **147**, 4448 (2000).

30. Z. He, L. Chen, B. Zhang, Y. Liu, and L. Fan, *J. Power Sources*, **392**, 232 (2018).

31. F. Langer, M. S. Palagonia, I. Bardenhagen, J. Glenneberg, F. L. Mantia, and R. Kun, *J. Electrochem. Soc.*, **164**, A2298 (2017).

32. J. R. Macdonald, *J. Chem. Phys.*, **61**, 15 (1974).